Discover Chemistry

Research

Adsorption of congo red from aqueous solution using rice husk, calcined kaolin clay, and microwaved rice husk clay hybrid

Abimbola O. Ige[1] · Babatunde O. Ogunsile[1] · Odunayo T. Ore[2] · David B. Olawade[3]

Received: 23 April 2024 / Accepted: 5 August 2024
Published online: 09 August 2024

Abstract
The present study focused on the comparative efficiency of rice husk (RH), calcined kaolin clay (CKC), and microwave rice husk clay hybrid (MRHCH) in the adsorption of congo red (CR) from aqueous solution. The rice husk was locally sourced and pulverized, the kaolin clay was calcined at 650 °C for two hours, while the rice husk clay hybrid was generated by microwave-impregnating an equal mixture of RH and CKC for 15 min at a medium temperature. The resulting adsorbents were characterized using scanning electron microscope (SEM) and Fourier transform infrared (FTIR) spectroscopy to evaluate their surface morphology and functional groups before and after adsorption. The effect of process variables comprising initial dye concentration, contact time, pH, and adsorbent dosage were investigated and the obtained adsorption equilibrium data were modelled using Langmuir, Temkin, and Freundlich isotherms. The adsorption kinetics were computed using Pseudo first order and Pseudo second-order reaction kinetics. The results of the study indicated that adsorption using all three adsorbents increased with increasing adsorbent dosage and contact time. On the other hand, adsorption using MRHCH and RH increased at a high initial concentration while CKC exhibited high adsorption at a low initial concentration. Isotherm studies indicated that Temkin isotherm best fits the adsorption equilibrium data while kinetic studies showed that the pseudo-second-order kinetic model best described CR adsorption, indicating chemisorption as the mechanism of adsorption. MRHCH demonstrated its exceptional adsorption capacity with a maximum adsorption capacity from the Langmuir isotherm of 4.008 mg/g. The adsorption process was found to be spontaneous, endothermic, and more random at the solid-solution interface by thermodynamic investigations. The study concludes that MRHCH has great promise for wastewater treatment applications as a very efficient adsorbent for CR removal.

Keywords Adsorption · Congo red · Isotherms · Kinetics · Thermodynamics

1 Introduction

One of today's most crucial and prevalent challenges is water pollution. Among pollutants, dyes are particularly harmful, mutagenic, and carcinogenic with devastating environmental impacts. Effluents from industries like textiles, paint, printing, photography, and pigment processing significantly increase total organic carbon (TOC) and biochemical oxygen demand (BOD) in rivers [1]. Dyes degrade water quality by preventing sunlight, slowing photosynthesis, inhibiting aquatic growth, and interfering with gas solubility [2]. The textile industry is a major polluter due to the vast amounts of water used in fabric processing, releasing highly visible coloured effluents. Annually, around 60,000 tons of dyes, primarily azo

✉ Odunayo T. Ore, oreodunayo@yahoo.com | [1]Department of Chemistry, University of Ibadan, Ibadan, Nigeria. [2]Department of Chemical Sciences, Achievers University, P.M.B. 1030, Owo, Nigeria. [3]Department of Allied and Public Health, School of Health, Sport and Bioscience, University of East London, London, UK.

dyes, are discharged into the environment [3]. Dye degradation produces carcinogenic chemicals causing skin, eye, and stomach irritation, respiratory issues, and sleep disturbances [4]. Specifically, Congo red (CR) breaks down into benzidine, a recognized human carcinogen, affecting the nervous system and bladder [5, 6]. The maximum permissible limit of CR in wastewater is set at 1 mg/L due to its toxic properties [7, 8]. The high toxicity of CR in wastewater poses a severe public health issue, prompting ongoing research and development of degradation strategies.

Chemical, physical, and biological methods are commonly used to remove dyes from industrial effluents. Chemical methods include coagulation-flocculation, ozonation, photocatalytic degradation, electrochemical therapy, and Fe^{2+} / $Ca(OH)_2$ precipitation-flocculation [9]. While effective, these methods can complicate sludge disposal and increase the risk of secondary pollution. Biological methods, in contrast, are environmentally friendly, energy-efficient, produce minimal sludge, and require little to no chemical intervention [10]. However, the synthetic and aromatic nature of dyes makes them difficult to degrade biologically [11]. Several methods, such as ozonation, adsorption, and advanced oxidation processes, have been adopted to remove synthetic dyes from aqueous systems. Among these, adsorption stands out due to its simplicity, effectiveness, low cost, high quality, ease of operation, insensitivity to harmful substances, and low running costs [12, 13]. Adsorption is particularly effective for non-biodegradable contaminants due to its simplicity and the availability of various adsorbents [14]. Adsorption can occur through van der Waals forces or electrostatic interactions, depending on the adsorbents and dyes' chemical composition [15]. Although activated carbon is the most commonly used adsorbent for dye removal, it is expensive to produce and regenerate [16].

The use of biological materials for dye removal from aqueous solutions, known as biosorption, has garnered significant interest as an eco-friendly alternative to traditional sorbents like activated carbon, ion-exchange resins, and inorganic materials such as silica gel, clay, zeolites, and activated alumina. Agricultural wastes such as rice husk, sugarcane bagasse, and corncobs, along with industrial wastes like coal ash, peat, clay, and bentonite, have been extensively studied for biosorption [17]. Rice husk, a low-cost by-product of the rice milling industry, consists of cellulose, hemicellulose, lignin, silica, and crude protein, making it an ideal adsorbent for metals and basic dyes [18]. It contains 32.24% cellulose, 21.34% hemicellulose, 21.44% lignin, 1.82% extractives, 8.11% water, and 15.05% mineral ash, with 94.5 – 96.34% SiO2 in the mineral ash [19]. Clay, with its nanometric size and layered structure, offers a large specific surface area for adsorption and is widely available. It has excellent chemical and mechanical stability, allowing it to retain a significant amount of natural and anthropogenic contaminants [20, 21].

Many recent exciting studies have reported the use of rice husk (modified and unmodified) as adsorbents in the removal of CR [19, 22–24]. Kaolin (modified and unmodified) has equally been widely adopted as an adsorbent in the removal of CR [25–28]. However, to the best of our knowledge, the use of rice husk and kaolin clay hybrid in the removal of CR from aqueous systems is yet to be reported. It has been suggested that the adsorption capacity of adsorbents can be increased through chemical, thermal, and physical treatments [29]. Hence, we attempted in the present study to impregnate rice husk and kaolin clay using microwave and evaluate its efficiency in the removal of CR from aqueous solutions. The efficiency of the rice husk, calcined kaolin clay, and microwaved rice husk kaolin clay hybrid were investigated under variable operating conditions of initial concentration, adsorbent dosage, and contact time.

2 Experimental

2.1 Adsorbents and adsorbate preparation

The rice husk (RH) was procured from the premises of the University of Ibadan, Nigeria, and 500 g of it was immersed in 98% purity 1 M NaOH solution supplied by Sigma-Aldrich for 24 h before being dried, ground, and sieved through 850 µm to create alkali-modified RH. The 95% purity Kaolin clay was obtained from SoundMind Chemicals in Ojota, Lagos State, calcined for two hours at 650 °C using a locally made furnace and sieved using 425 µm. Modified calcined clay and modified rice husk were combined in a 1:1 ratio and microwaved for 15 min at medium temperature to generate MHRCH. Congo red of high analytical quality of 99% was purchased from Sigma-Aldrich (Molecular Weight: 696.66 g/mol; molecular formula of $C_{32}H_{22}N_6Na_2O_6S_2$; Color Index Number: 22,120 and λ_{max} of 497 nm). In order to make the CR stock solution (1000 mg/L), 1 g of CR was dissolved in 1 L of distilled water. For the experiment, the working solutions were prepared from the stock by serially diluting the stock to various concentrations.

2.2 Design of experiment and influence of process parameters

The effects of process parameters comprising adsorbent dosage, contact time, and pH, initial concentration were investigated in this study. The adsorbent dosage was taken at 0.1, 0.2, 0.3, 0.4, 0.5, 0.75, and 1 g for 48 h in 100 mg/L CR solution. In addition, contact times of the adsorbents with 100 mg/L CR solution at 2, 5, 10, 20, 30, 60, 120, and 240-min intervals and the initial concentrations of 50, 100, and 150 mg/L were used to monitor the influence of time and concentration on the adsorption experiment while initial pH solutions of 3, 5, 7, and 9 were used to study the effect of pH. The adsorbents were weighed and added to 25 mL of 100 mg/L CR solution and this was agitated on a Thermostated Shaker Bath for 48 h. At the end of the adsorption experiments, the unadsorbed CR solution was separated from the adsorbent by centrifuging. The concentration of the unadsorbed dye in the filtrate solution was measured at 497 nm using a UV spectrophotometer.

The amount of dye adsorbed and the percentage of dye adsorption were calculated according to Eqs. (1) and (2) respectively [30]:

$$Q_e = \frac{(C_o - C_e) \times V}{M} \tag{1}$$

$$\%removal = \frac{C_o - C_e}{C_e} \times 100 \tag{2}$$

where Co and Ce are the initial and equilibrium concentrations of the dye respectively, V is the volume of the solution (L), and M is the weight of the adsorbent (g).

2.3 Adsorption isotherm and kinetics

The temperature and concentration-dependent data were subjected to Langmuir, Freundlich, and Temkin isotherm models which are presented in Eqs. (3–5) respectively.

$$\frac{\text{Ce}}{\text{qe}} = \frac{1}{\text{qmKe}} + \frac{\text{Ce}}{\text{qm}} \tag{3}$$

where C_e stands for the adsorbate concentration at equilibrium (mg/L), q_e is the amount adsorbed on the unit mass of adsorbate (mgg^{-1}) and q_m is the amount of adsorbate necessary to create a monolayer on the unit mass of adsorbate. The monolayer adsorption capacity, q_m, and adsorption equilibrium constant, b, can be determined from the equation of the graph by plotting $1/q_e$ versus $1/C_e$, which results in a straight-line graph.

$$\text{Log qe} = \text{LogKf} + \frac{1}{\text{n}}\text{Log Ce} \tag{4}$$

where C_e is the adsorbate's equilibrium concentration (mg/L), q_e stands for the amount adsorbed (mg/g), and K_F and n are the Freundlich constants for capacity and intensity, respectively. The Freundlich parameters n and K_F are calculated using linear graphs of log q_e against log C_e.

$$q_e = BLnK_T + BLnC_e \tag{5}$$

where B = RT/b, b is Temkin's constant, K_T is the Bound Equilibrium Constant (L g^{-1}), and B is related to the heat of adsorption (J mol^{-1}). From the linear plot of q_e against Ln C_e, the parameters B and K_T are calculated.

The time-dependent data was subjected to pseudo-first-order and pseudo-second-order kinetics and this is shown in Eqs. 6 and 7 respectively:

$$\log(\text{qe} - \text{qt}) = \log \text{qe} - \frac{\text{k1}}{2.303}\text{t} \tag{6}$$

$$\frac{\text{t}}{\text{qt}} = \frac{1}{\text{k2qe2}} + \frac{1}{\text{qe}}\text{t} \tag{7}$$

where the amounts of dye adsorbed on the adsorbent at equilibrium and time t (min), are denoted by q_e and q_t (mg/g) respectively. Adsorption rate constant k_1 (min) is also used and k_2 is the rate constant for the pseudo-second order kinetic model. Also, the thermodynamic study is conducted using the values from the adsorption isotherms parameters.

2.4 Characterization of adsorbents

The adsorbents functional groups were examined using a Fourier transform infrared (FT-IR) spectrophotometer (Spectrum One, Perkin Elmer, USA) with a wavelength range of 4000 – 400 cm^{-1} before and after adsorption, as reported by [31]. Before FT-IR analysis, the adsorbents were produced by combining them with potassium bromide (KBr) and compressing them into pellets. The scanning electron microscope (SEM) was used to examine the surface morphology of the adsorbents. The samples for SEM examination were coated with a thin layer of gold to improve conductivity and the quality of the image.

3 Results and discussion

3.1 Characterization of adsorbents

Fourier transform infrared (FT-IR) spectroscopy provides information about the available active sites on an adsorbent's surface which can interact or bind with the molecules of a pollutant [32]. The FT-IR spectra of rice husk, calcined kaolin clay, and microwaved rice husk kaolin clay hybrid are shown in Fig. 1. The FTIR spectra of the rice husk adsorbent exhibited a peak at 3455 cm^{-1} for both the untreated rice husk (RH) and the rice husk after being treated with CR (RHC), suggesting the existence of hydroxyl (-OH) groups in both samples. It was observed by [33] that the peaks at 1731.7 and 1636.9 cm^{-1} are associated with the stretching of carbonyl groups in aldehydes and ketones, respectively. The rice husk adsorbent displays lignocellulosic absorption bands at specific wavelengths (794, 1033, 1457, 1511, 1635, 2916, 3312, and 3748 cm^{-1}) both before and after adsorption, with negligible differences. The presence of Si–O bonding is shown by the peaks at 794 and 1033 cm^{-1} [34]. The observed reduction in the intensity of the wide peak in the range of 3300–3500 cm^{-1} in the sample treated with CR indicates the potential formation of hydrogen bonds between the OH groups on rice husk and CR molecules. This shows that there is an interaction between CR and the cellulose, hemicellulose, or lignin components found in rice husks. Interactions between CR and rice husk components may cause shifts in peak positions within the 2800–3000 cm^{-1} range, indicating alterations in the molecular environment. Interactions between CR and lignin may be suggested by comparable shifts within the 1700–1750 cm^{-1} range. The emergence of additional peaks may suggest the occurrence of contacts between the azo group (N=N) or sulphate groups (SO_3^-) in CR and the hydroxyl groups (OH) on cellulose, hemicellulose, or lignin through hydrogen bonding or electrostatic interactions. The FTIR spectrum provides evidence of pi-pi stacking interactions between the aromatic rings in CR and the aromatic structures in lignin.

After CR adsorption, CKC and CKCC FTIR spectra showed increased transmittance percentage intensity, suggesting surface changes. The broad band at 3468 cm^{-1} is due to the OH vibration mode of the hydroxyl molecule (Al–OH or Si–OH) in kaolin. The broad band at 1039 cm^{-1} indicates Si–O and Al-O stretching vibrations, indicating siloxane and aluminate groups in clay composition. A tiny peak at 2345 cm^{-1} suggests hydroxyl deformation from water molecules, adding to the spectrum.

FTIR spectra changed after CR adsorption. Reduced intensity of O–H stretching peak at 3620–3670 cm^{-1} shows probable hydrogen bonding between kaolinite and CR molecules. The observed intensity reduction may be due to this interaction limiting O–H group vibrational freedom. CR may interact with siloxane (Si–O) groups in kaolinite, as indicated by peak position shifts about 1000–1200 cm^{-1} for Si–O stretching. The azo or sulphate groups in CR may interact with the hydroxyl groups (O–H) on the borders of kaolinite layers through hydrogen bonding or electrostatic interactions. These peak positions and intensities suggest new CR-CKC complexes that affect surface functional group vibrations. Novel peaks in the red line spectrum may suggest novel chemical species from adsorption. The observed spectrum variations reveal the role of particular functional groups in CR adsorption onto CKC [35].

In the MHRCH spectrum, stretching vibration at the adsorbent surface before adsorption is greater than after adsorption, indicating a drop in transmittance % intensity. This implies CR molecules have occupied the adsorbent's surface. The drop in peak intensity at 3445 cm^{-1} suggests that CR adsorption impacts O–H stretching vibrations on the surface, possibly from cellulose, hemicellulose, or kaolinite. CR molecules contact the functional groups on MHRCH by hydrogen bonding between the O–H groups and the azo groups (N=N) or sulphate groups (SO_3^-), reducing peak intensity and

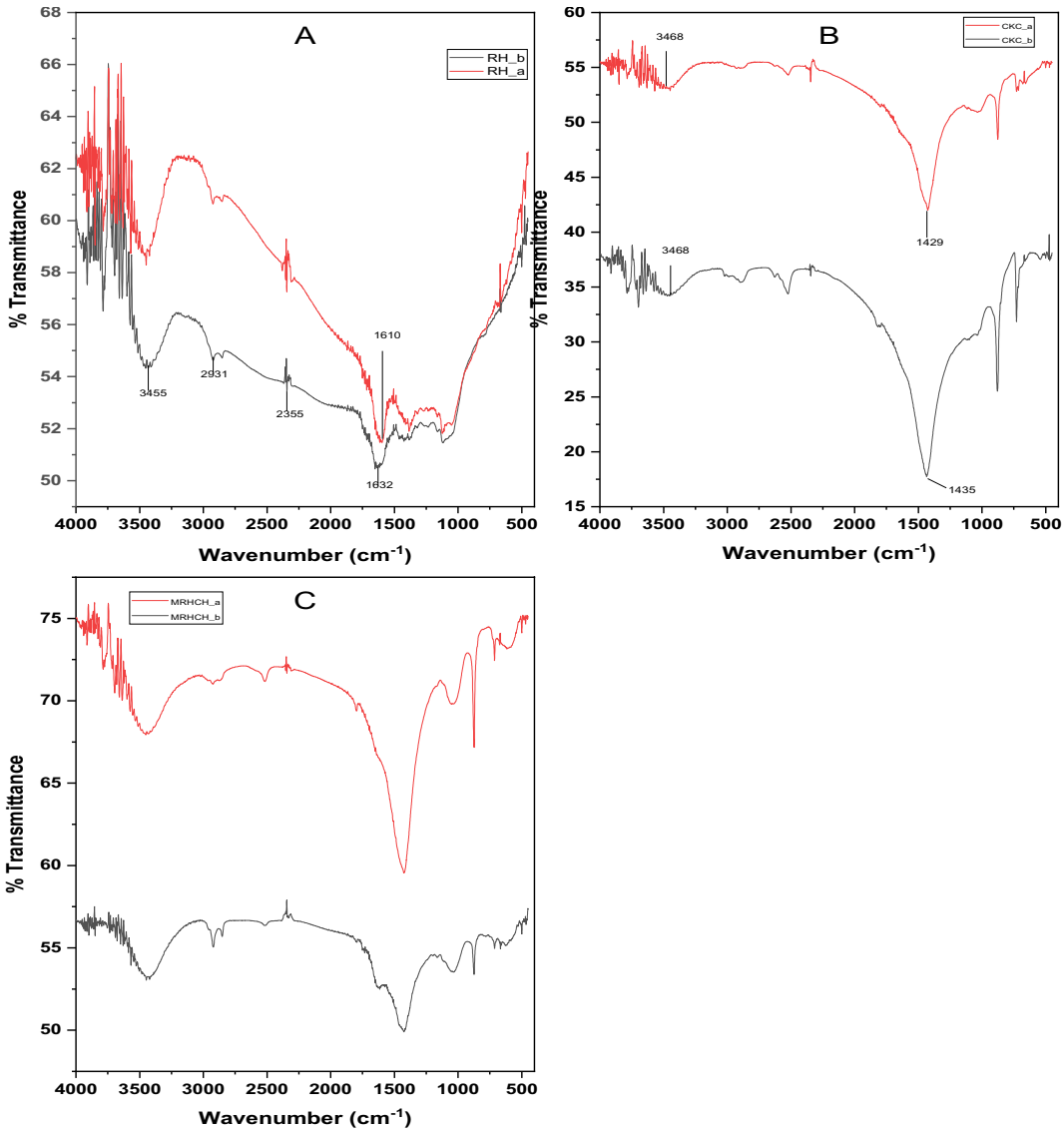

Fig. 1 FTIR spectra of **A** RH, **B** CKC, and **C** MRHCH adsorbents before and after adsorption of CR dye

showing surface coverage. The peaks at 2924 cm^{-1} and 3445 cm^{-1} indicate the stretching vibrations of C–H and –O–H groups, confirming the involvement of functional groups in adsorption [36].

For all three adsorbents, it was observed that their basic structures remained unchanged before and during adsorption except for some slight variations in the absorption intensities of some functional groups. This observation is consistent with previous findings [37, 38]. The minimal variations in absorption intensities after adsorption are probably due to the increased presence of adsorbed dye molecules which may have slightly affected the interaction of surface functional groups of the dyes with the adsorbent. This interaction could occur either via van der Waals forces or electrostatic interaction owing to the physical interaction of adsorbent dyes at the surface and/or the ionic properties exhibited by the dyes in solution [39, 40]. Furthermore, the variations in absorption intensity before and after adsorption reflect the adsorption loads. For all three adsorbents, the absorption intensity is characterized by a relative decrease after adsorption, suggesting that the adsorbent's surface has been occupied by the dyes and this may block the infrared signal [37].

Scanning electron microscopy (SEM) is a method employed to observe the structures of materials, offering crucial data regarding the dimensions and forms of particles. Figure 2 displays the SEM images of the adsorbents. The adsorbents exhibit rough surface patterns characterised by prominent gaps and irregular folds, which function as active sites for the removal of dyes. The micrograph for MRHCH reveals a surface that is porous and lacks homogeneity. The outer epidermis

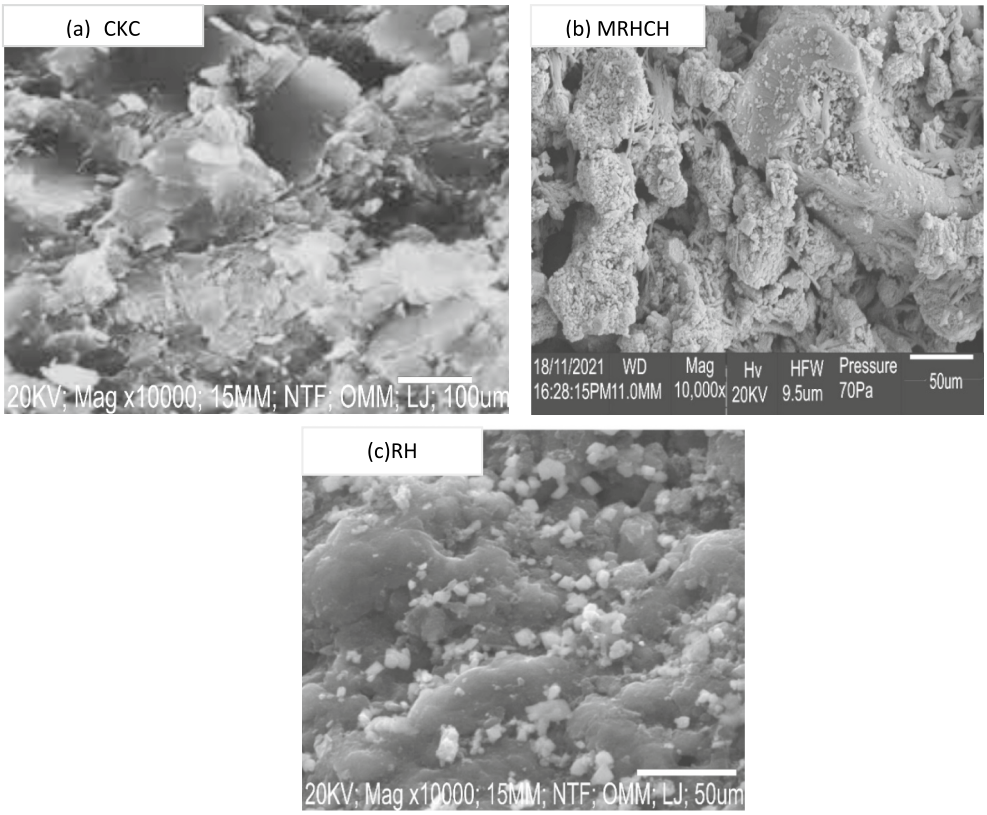

Fig. 2 SEM images of **a** CKC, **b** MRHCH and **c** RH adsorbents prepared by respective modification and calcination processes

appears ruptured with obvious fissures, far more distended than in other adsorbents. The fractured surface and porous structure of this material can generate an ideal condition for the binding of molecules.

Similarly, the image of calcined kaolin clay (CKC) displays plate-like structures that indicate the layered composition of kaolinite, the main mineral. Calcination causes the removal of hydroxyl groups and the disintegration of the material, leading to the formation of uneven plates with coarse surfaces, as observed in the scanning electron microscopy (SEM) analysis conducted by [41]. These modifications enhance the accessible surface area for Congo red adsorption, with proof of particle aggregation resulting from sintering during calcination. Electrostatic interactions and hydrogen bonding have the potential to increase the adsorption capacity even more. Moreover, the scanning electron microscopy (SEM) examination of rice husk (RH) reveals sturdy, elongated formations with a coarse and uneven surface, which can be attributed to the presence of cellulose fibres and silica deposits. Cellulose fibres, which have a rod-like form, are a fundamental constituent of the cell wall [42]. Additionally, there are irregularly shaped particles present, which suggest that they are fragmented silica phytoliths.

3.2 Influence of process parameters

3.2.1 Effect of adsorbent dosage

The adsorbent dosage conveys information for optimization and design purposes since it shows how the adsorbate interacts with the adsorbents. The variation in percentage adsorption with respect to adsorbent dosage is shown in Fig. 3. Each adsorbent had a similar pattern in terms of the adsorbent's efficiency and capacity for adsorption. The amount of CR adsorbed per unit weight of adsorbent decreases as adsorbent dosage is increased. It was observed that the q_e (mg/g) decreases (23.8 to 2.4 for MRHCH, 12.7 to 2.4 for CKC, and 16.7 to 2.2 RH) as the adsorbent dose increases. The fundamental reason for this was that when adsorbent dosage increased, the surface area and effective adsorption sites increased, improving the removal rate under constant CR concentration [43]. Beyond 0.75 g of the adsorbent, the percentage removal of the dye seems fairly constant, suggesting that 0.75 g is the optimal adsorbent dosage. MRHCH was more efficient than CKC and RH. Under the same conditions, MRHCH, CKC, and RH exhibited

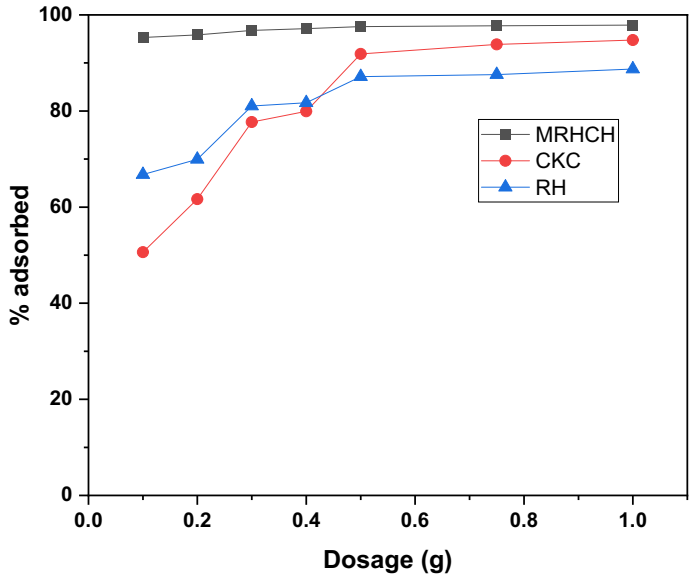

Fig. 3 Effect of adsorbent dosage of MRHCH, RH and CKC ranging from 0.1 g to 1 g in 100 mg/L CR solution for 48 h

98, 95, and 89% removal of CR dye respectively. The marked differences in dye removal exhibited by the adsorbents could be due to differences in surface morphology and adsorbent-dye interactions [44].

3.2.2 Effect of contact time

In adsorption tests, contact time affects sorption kinetics [45]. Figure 4 shows how contact time affects CR removal by the three adsorbents. The plot shows that CR adsorption increases with the contact time, indicating that the adsorbent's active sites were initially unoccupied with enough CR dye in the solution [39]. The qe for MHRCH increased rapidly from 15.64652 mg/g at 2 min to 18.55823 mg/g at 60 min, and further to 20.2176 mg/g at 180 min. For RH, the qe increased from 0.71541 mg/g at 2 min to 3.86792 mg/g at 60 min, reaching 5.09434 mg/g at 180 min. Similarly, for CKC, q_e increased from 1.97326 mg/g at 2 min to 4.02706 mg/g at 60 min, and then to 5.04994 mg/g at 180 min. For MHRCH, the q_e increases sharply and reaches a relatively stable value after about 60 min. This implies that MHRCH adsorption increases minimally after 60 min of contact. Thus, the MHRCH equilibrium contact time is 60 min. Similar to RH and CKC, their adsorption capabilities stabilize after 60 min, indicating an equilibrium contact period of 60 min. Adsorption increased with time for all adsorbents, suggesting they had unoccupied active sites that gradually filled.

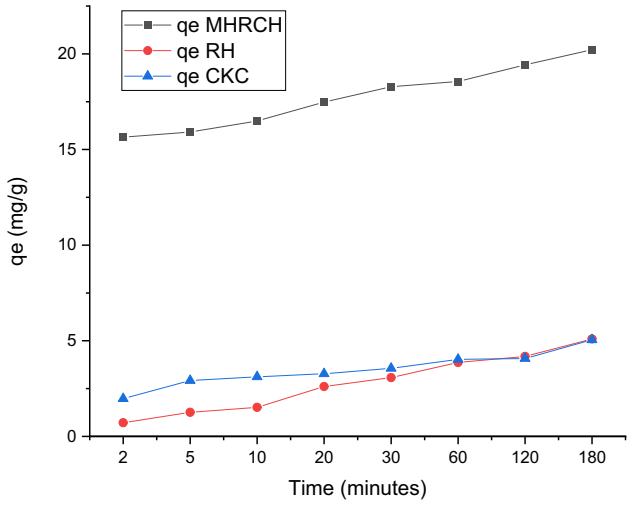

Fig. 4 Effect of contact time on 100 mg/L CR removal by MRHCH, RH and CKC at 0.1 g dosage from 2 to 180 min

Due to its higher porosity, active sites, and surface area, MHRCH had the greatest q_e of the adsorbents evaluated. The optimal and equilibrium contact time for MHRCH, RH, and CKC CR dye adsorption is 60 min, beyond which adsorption capacity does not increase.

3.2.3 Effect of concentration

Congo Red adsorption was investigated at 150, 100, and 50 mg/L starting concentrations. Adsorption capabilities were measured up to 180 min, showing unique trends for each adsorbent. High MRHCH adsorption capacity at 100 mg/L indicates excellent Congo Red interaction for efficient adsorption. Previous investigations have shown that greater starting concentrations increase mass transfer driving force and adsorption rates [46]. RH also adsorbed well at 100 mg/L, showing strong dye-adsorbent interactions. According to [47], higher starting concentrations increase adsorption capability because more adsorbate molecules are available. Lower quantities of CKC remove dye more efficiently, suggesting a higher affinity for CR. It was observed by [48] that higher affinity binding sites make some adsorbents function better at lower concentrations. The study found that MRHCH and RH have better adsorption capabilities at 100 mg/L, indicating excellent interaction and effective adsorption (Fig. 5). The Langmuir and Freundlich isotherm models demonstrate that larger starting concentrations increase adsorption efficiency by increasing mass transfer driving force and favourable adsorption conditions. According to the Temkin isotherm model, CKC has higher affinity binding sites at 50 mg/L. These findings show that initial dye concentration is crucial to water treatment adsorption efficacy.

3.2.4 Effect of pH

The pH plays an important role in the adsorption process, influencing the surface charge of adsorbents [49]. Specifically, the adsorption efficiency of anionic dyes increases as the pH of the dye solution decreases [50]. The three adsorbents were used for the adsorption of CR at pH values of 3, 5, 7, and 9. The effect of pH on CR adsorption is shown in Fig. 6. The removal efficiencies were found in the range of 87–98%, 76–86%, and 87–97% for MRHCH, CKC, and RH respectively. For all three adsorbents, the highest removal efficiencies were achieved at pH range 3–5. Protonation occurs when adsorbents gain a positive charge in an acidic solution. This process improves the adsorption of the negatively charged CR dye. As a result, the electrostatic attraction between the negatively charged CR and the positively charged adsorbent increases. This is consistent with similar studies in the literature where it was suggested that the acidic pH range favours the adsorption of CR [51, 52].

3.3 Adsorption isotherm

Langmuir, Freundlich, and Temkin isotherm models were used to study MRHCH, CKC, and RH adsorption. The parameters are in Table 1 while the isotherm plots are presented in Fig. 7. The regression coefficient (R^2) was highest for the Temkin isotherm across all adsorbents, demonstrating the best fit to experimental data. The Freundlich and Temkin isotherms had equal R^2 values, but the Temkin model had maximum R^2 values for all adsorbents, suggesting that it fits the data better [53, 54]. The negative values of bT for all adsorbents indicate an exothermic adsorption process that releases heat [55]. The greatest bT value among adsorbents is MRHCH, indicating energy efficiency. Other indicators like qm and kf reveal adsorption capacity and intensity. MRHCH has the greatest qm value, outperforming CKC and RH in adsorption. Conversely, RH had the highest k_f value, indicating more adsorption. The Temkin isotherm proposes that the heat of adsorption decreases linearly as coverage increases, offering a more accurate description of adsorbent-adsorbate interactions in certain cases. This assumption is especially relevant to chemisorption processes, where interactions have significance [56]. The Freundlich isotherm, on the other hand, is empirical and better suited to describe adsorption on heterogeneous surfaces, meaning that adsorption heat is not distributed uniformly.

3.4 Adsorption kinetics

The adsorption kinetics were assessed to ascertain the rate-controlling processes and the mechanism of adsorption [57]. Table 2 and Fig. 8 demonstrate that the adsorption of CR onto MRHCH, CKC, and RH adsorbents is mostly governed by the pseudo-second-order kinetic model. The finding is substantiated by the strong correlation values (R2 = 1) and the close concordance between the estimated and experimental qe values. In contrast, the pseudo-first-order model exhibited lower R2 values, suggesting that it is not a suitable fit for characterising the adsorption kinetics of the sorbents.

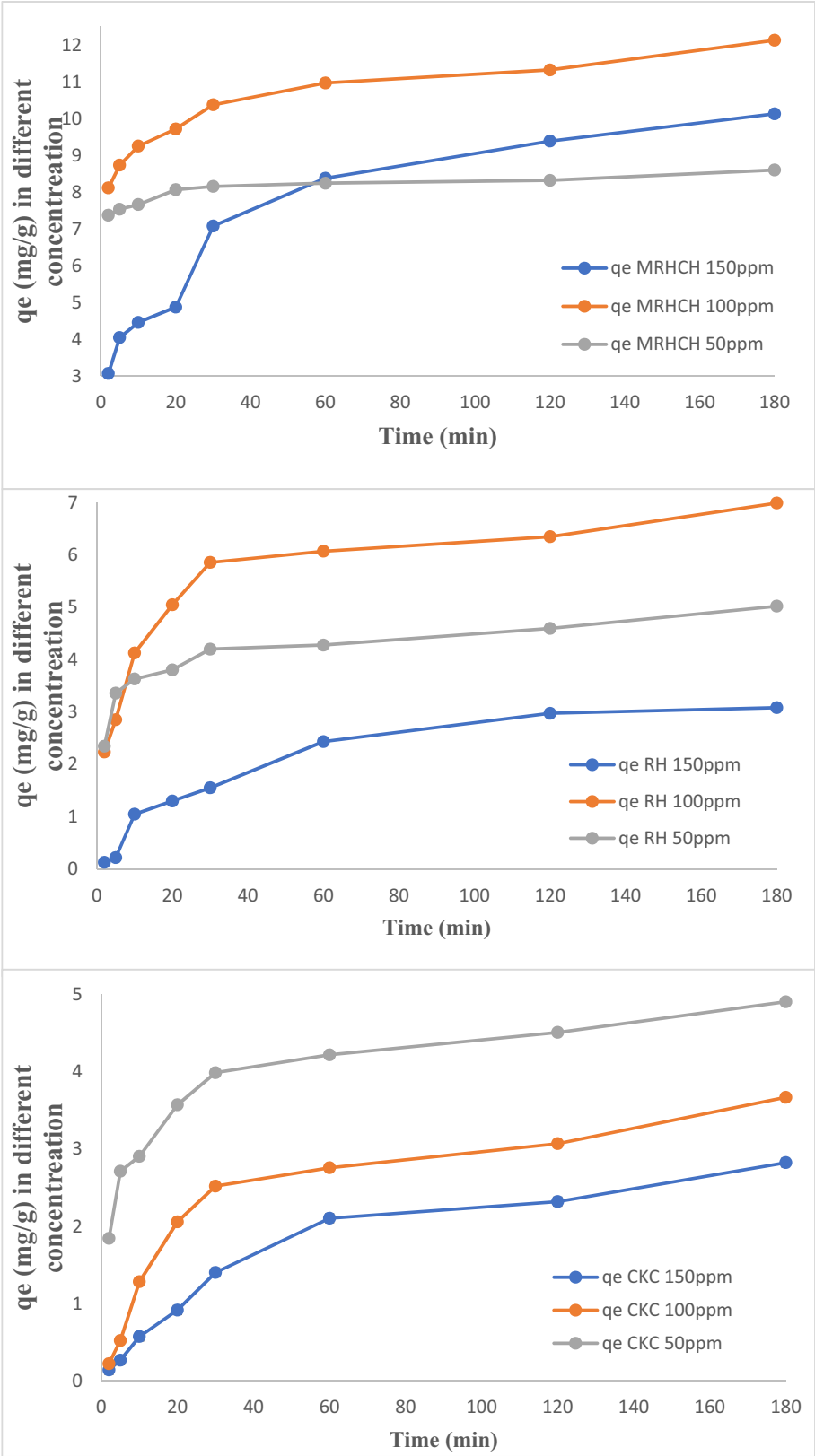

Fig. 5 The removal efficiency of CR at different initial concentrations (50 mg/L, 100 mg/L, and 150 mg/L) using MRHCH, RH and CKC at 0.5 g dosage

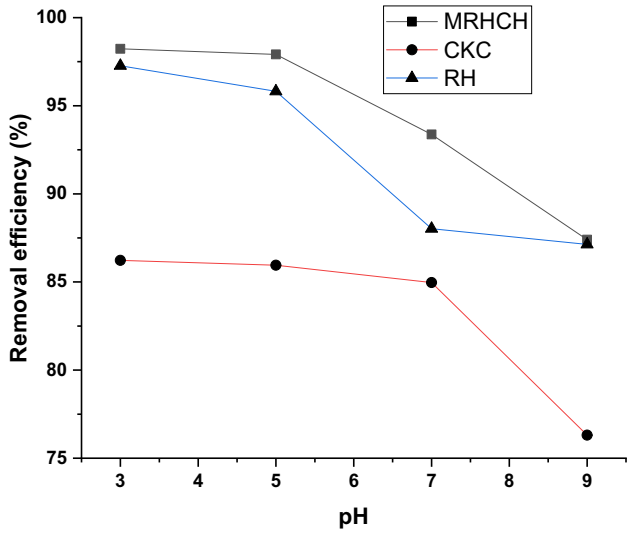

Fig. 6 Effect of pH on the adsorption of Congo red by MRHCH, CKC, and RH

Table 1 Data for the equilibrium isotherm of the CR adsorption onto MRHCH, CKC, and RH

Adsorbent	Langmuir			Freundlich			Temkin		
	q_m (mg g^{-1})	b	R^2	n	k_f (L/mg)	R^2	K_T (L/g)	b_T (J/mol)	R^2
MRHCH	4.008	0.311	0.932	4.340	9.836	0.982	0.00069	− 2140.82	0.988
CKC	2.194	3.974	0.973	1.462	46.355	0.993	0.00570	− 981.45	0.997
RH	0.883	0.027	0.900	0.619	1790.61	0.974	0.00870	− 653.782	0.996

The superior fit of the pseudo-second-order model indicates that the adsorption process is probably determined by chemisorption, which involves the exchange or sharing of electrons between the adsorbate and adsorbent [45, 58]. These findings align with other research that has shown the prevalence of the pseudo-second-order model in adsorption processes, providing further confirmation of the chemisorptive character of the interactions involved [57, 59–61]. The results of the adsorption kinetics show that the adsorption of CR onto MRHCH, CKC, and RH is governed by a chemisorption mechanism. This is supported by the successful fitting of the pseudo-second-order model to the experimental data.

3.5 Thermodynamic study

The thermodynamic characteristics of MRHCH, CKC, and RH exhibit distinct adsorption behaviours. The thermodynamic parameters for the adsorption of congo red adsorption are presented in Table 3. The adsorption of MRHCH is characterised by a lack of spontaneity and the release of heat, accompanied by a decrease in disorder. This is evidenced by a positive ΔG° and a negative ΔS° [62]. On the other hand, CKC exhibits spontaneous and exothermic adsorption, characterised by a rise in disorder, as evidenced by a negative ΔG° and a positive ΔS° [37]. Similarly, the RH exhibits non-spontaneous and exothermic adsorption, characterised by a decrease in randomness, as indicated by a positive ΔG° and a negative ΔS°.

3.6 Comparison of state-of-the-art techniques and comparative analysis of adsorption performance for various dyes and adsorbents

With better efficiency and different thermodynamic features, Congo red adsorption has improved significantly and the study is compared to other previous studies on adsorption performance as shown in Table 4.

The removal efficiencies reported in the present study were relatively better than other adsorbents reported in the literature owing to the following reasons:

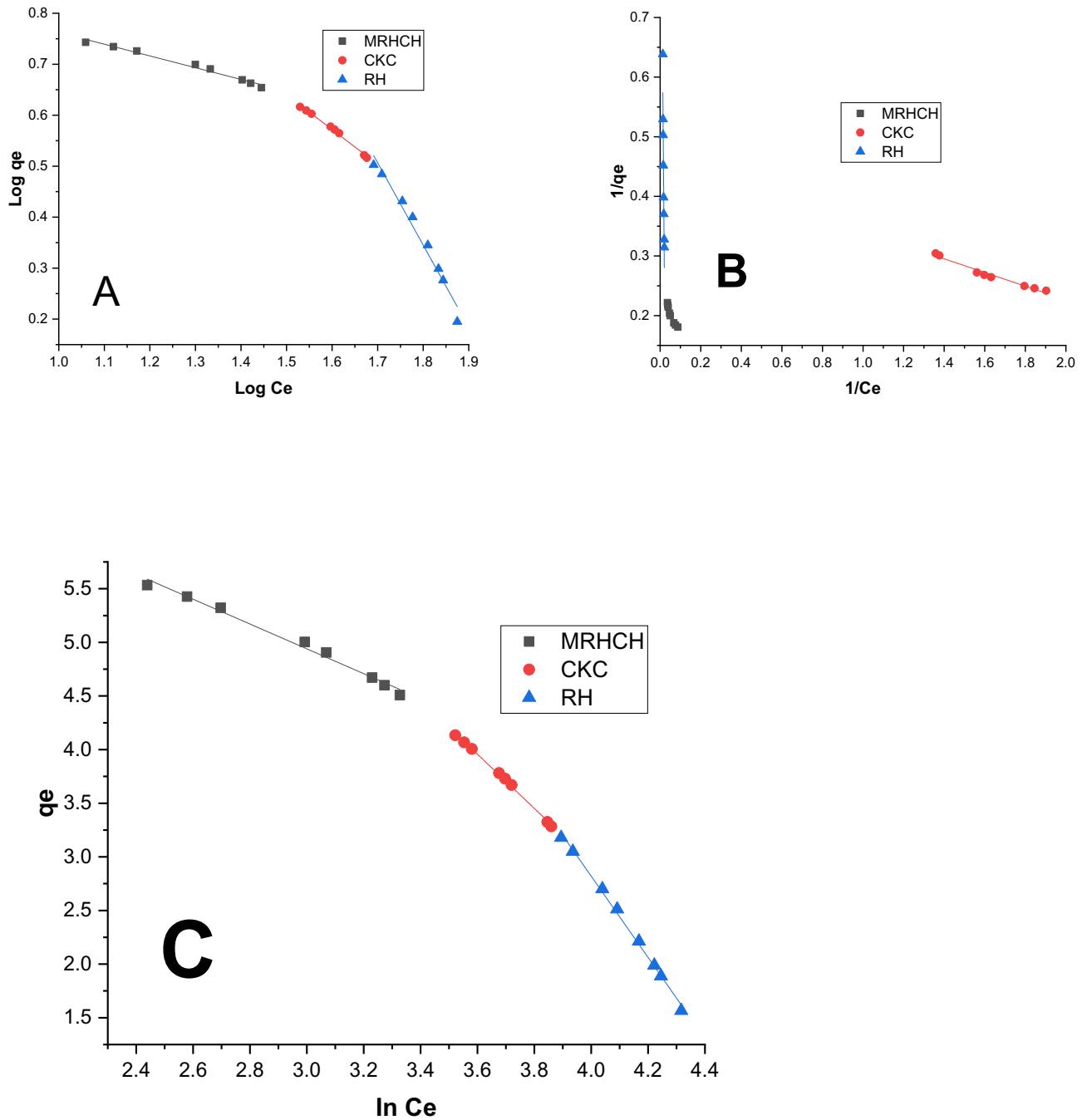

Fig. 7 Adsorption isotherms **A** Freundlich, **B** Langmuir, and **C** Temkin plots for the adsorption of 100 mg/L CR using MRHCH, CKC, and RH

Table 2 Parameters of pseudo-first and second order for the adsorption of CR on MRHCH, CKC, and RH

Adsorbent	Pseudo-first order equation			Pseudo-second order equation			
	q_{e1}	K_1	R^2	q_{e2}	K_2	R^2	Experimental q_e
MRHCH	0.988	– 0.009	0.9621	5.562	0.090	0.9997	5.534
CKC	0.853	– 0.009	0.9251	4.153	0.139	0.9998	4.134
RH	1.182	– 0.009	0.9863	3.247	0.046	0.9972	3.180

Fig. 8 Pseudo-second-order plots for the adsorption of 100 mg/L CR onto 0.4 g **a** CKC, **b** MRHCH, and **c** RH monitored over contact time from 2 to 180 min

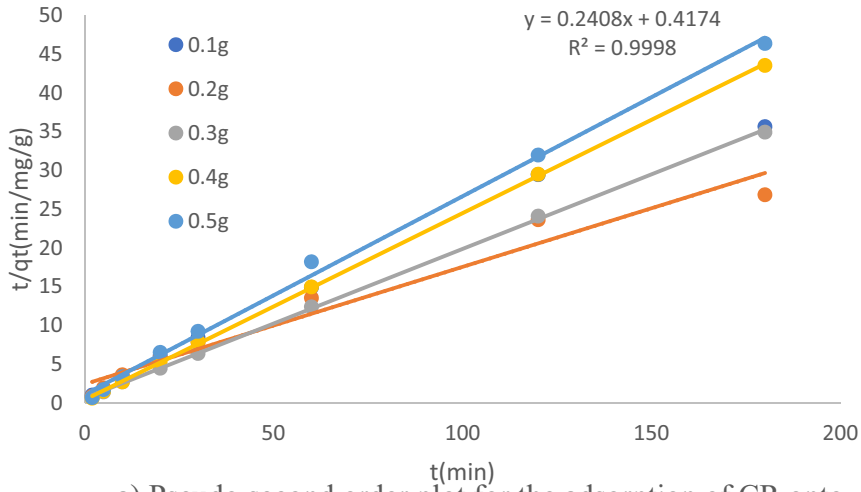

a) Pseudo second order plot for the adsorption of CR onto CKC.

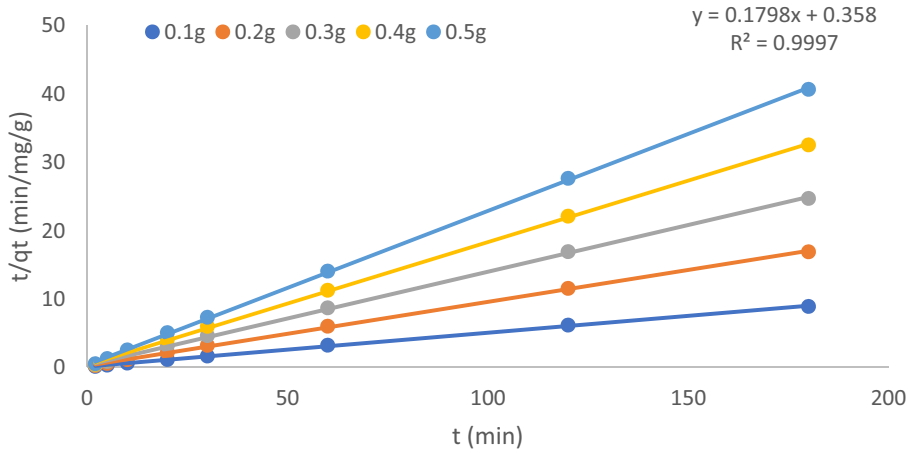

b) Pseudo second order plot for the adsorption of CR onto MRHCH.

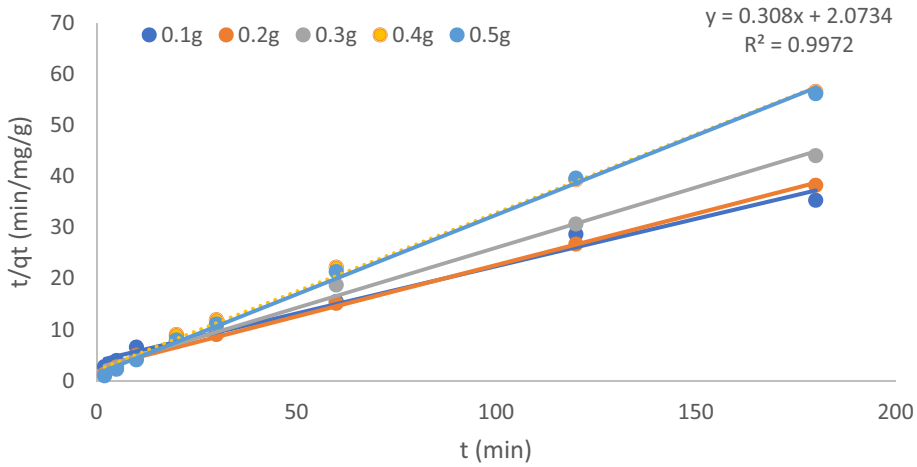

c) Pseudo second order plot for the adsorption of CR onto RH.

Table 3 Thermodynamic Parameters for Adsorption of CR Dye

Adsorbent	Langmuir Constant b (L/mg) or Equilibrium Constant KL	Gibbs Free Energy Change ΔG° (kJ/mol)	Temkin Constant KT (L/g)	Temkin Constant bT (J/mol)	Enthalpy Change ΔH° (kJ/mol)	Entropy Change ΔS° (J/mol·K)
MRHCH	0.311	2.89	0.00069	– 2140.82	– 2.14	– 16.87
CKC	3.974	– 3.42	0.00570	– 981.45	– 0.98	8.19
RH	0.027	8.96	0.00870	– 653.782	– 0.65	– 32.24

1) Enhanced Adsorption: Overtaking activated carbon, MRHCH had the maximum adsorption capacity (98%), followed by CKC (95%) and RH (89%). The improved performance can be due to MRHCH's superior surface characteristics, which were boosted via heat treatment and microwave-assisted preparation. These enhancements most likely resulted in increased surface area, porosity, and more active adsorption sites.
2) Thermodynamic Properties: MRHCH and RH imply exothermic, non-spontaneous adsorption with decreased randomness (positive ΔG° and negative ΔS°). Positive ΔS° and negative ΔG° suggest spontaneous, exothermic adsorption in CKC with increasing unpredictability. Congo red may interact differently due to these features. These thermodynamic features imply that different adsorbents have varied interactions with CR, which can be tailored to specific application conditions.
3) Kinetic/Isotherm Models: With increased surface covering, the binding energy is evenly distributed and adsorption heat decreases, according to the Temkin model. Following pseudo-second-order kinetics, chemisorption was found to be the rate-limiting phase and this indicates stronger adsorption interactions. The Temkin model provides a more detailed knowledge of the energy changes that occur during adsorption, which, when combined with kinetic analysis, aids in fine-tuning the process for optimal efficiency.
4) Advanced Adsorbent Preparation: Thermally treated microwaved rice husk clay hybrid (MRHCH) improves surface characteristics such as surface area and pore size, as well as Congo red adsorption effectiveness. This method may work for advanced water treatment utilising agricultural waste.

4 Conclusion

The study delved into the potential for adsorption of congo red (CR) using rice husk (RH), calcined kaolin clay (CKC), and microwaved rice husk clay hybrid (MRHCH). The highest removal efficiency was achieved by MRHCH (98%), followed by CKC (95%), and RH (89%). As contact time increases, the removal efficiency rises. While MRHCH and RH gave the best adsorption at 100 mg/L, the adsorption capacity of CKC decreased at higher concentrations. The isotherm data was best fitted into the Temkin isotherm model which denotes an even distribution of binding energy, characterizes adsorption and the rate at which the adsorption heat of all molecules declines with increasing coverage of the adsorbent surface. The kinetic study followed the pseudo-second-order kinetics with very high correlation coefficients. The calculated values of q_e were also close to the experimental data. In consonance with existing evidence in the literature, the present study further confirmed that the efficiency of adsorbents can be increased by thermal treatment owing to the greater adsorption efficiency exhibited by the microwaved rice husk clay hybrid adsorbent. It is suggested that the impact of different types of thermal treatment on the efficiency of adsorbents should be further investigated. Also, the use of other agricultural wastes as potential adsorbents should be explored in future studies. Finally, the feasibility and effectiveness of these adsorbents in real-world applications should be evaluated.

Table 4 Comparative Analysis of Adsorption Performance for Various Dyes and Adsorbents

Adsorbate-adsorbent relationship (citation)	Adsorption performance	Adsorption isotherm model	Maximum adsorption capacity	Adsorption kinetics model
Congo red (CR)—Activated carbon from Bombax Buonopozense (AC-BBP) [11]	Removal efficiency of 86.12% at optimal conditions (adsorbent dose: 0.117 g/L, pH: 7.87, contact time: 29 min)	Langmuir	510.2 mg/g	Pseudo-second-order
Reactive Black 5 (RB5), Cong Red (CR)—Banana Peel Powder (BPP) [40]	Highly efficient adsorption of dyes, notably Cong Red (CR), with excellent capacity and kinetics	Langmuir	49.2 mg/g (RB5), 164.6 mg/g (CR)	Pseudo-second-order
Cationic red 14 dye—Cherry wood activated carbon (CWAC) [12]	Increased efficiency at higher contact times, temperatures, and pH. Decreased at higher initial dye concentrations	Langmuir	Highest removal efficiency at optimal conditions: pH = 11, time = 45 min, dye concentration = 50 mg/L, AC dose = 0.25 g/L	Pseudo-second-order
Congo Red—Indonesian rice husk biochar (RH-BC), pristine rice husk (RH) [23]	Pyrolysis temperature (500 °C), surface-area-specific analysis	Freundlich	72.993 mg/g (RH), 85.470 mg/g (RH-BC)	Pseudo-second-order
Cephalexin—Magnetized activated carbon ($CoFe_2O_4$) [63]	Removal efficiency decreases with higher pH and initial concentration	Freundlich	27.5 mg/g at 0.25 g/L, decreases to 18.3 mg/g at 2.5 g/L	Pseudo-second-order
Congo red (CR) dye—MoS_2 nanopowder [5]	Excellent decolorization property	Langmuir	80.64 mg/g at 50 °C	Pseudo-second-order
Eosin Y (Eo-Y) and Erythrosine B (Er-B)—ZnO-NPs doped on activated carbon (AC-ZnO) [64]	High removal efficiency: 95.11% for Eo-Y and 98.31% for Er-B	Langmuir	163.9 mg/g for Eo-Y, 144.92 mg/g for Er-B	Pseudo-second-order
Congo red—microwave rice husk clay hybrid (MRHCH), calcined kaolin clay (CKC), and rice husk (RH) [Present study]	MRHCH, CKC, and RH exhibited 98, 95, and 89% removal efficiency	Temkin	4.008 mg/g	Pseudo-second-order

Acknowledgements The authors sincerely acknowledge the management of the University of Ibadan, Ibadan, Nigeria for providing an enabling environment for the research.

Author contributions BOO—designed and conceived the study AOI—conducted the experiments OTO and DBO—wrote the main manuscript All authors reviewed the manuscript.

Data availability The authors declare that the data supporting the findings of this study are available within the paper and its Supplementary Information files. Should any raw data files be needed in another format they are available from the corresponding author upon reasonable request.

Declarations

Competing interests The authors declare that there is no conflict of interest.

References

1. Ogunsile B, Bamgboye M. Sorption characteristics of methylene blue onto Nypafruiticans lignin. IFE J Sci. 2017;19(2):201–15.
2. Dutta S, Gupta B, Srivastava SK, Gupta AK. Recent advances on the removal of dyes from wastewater using various adsorbents: a critical review. Mater Adv. 2021. https://doi.org/10.1039/d1ma00354b.
3. Liu Q. Pollution and treatment of dye waste-water. IOP Conf Series. 2020;514: 052001. https://doi.org/10.1088/1755-1315/514/5/052001.
4. Roy TK, Mondal NK. Potentiality of Eichhornia shoots ash towards removal of Congo red from aqueous solution: isotherms, kinetics, thermodynamics and optimization studies. Groundw Sustain Dev. 2019;9: 100269. https://doi.org/10.1016/j.gsd.2019.1002690.
5. Alarifi IM, Al-Ghamdi YO, Darwesh R, Ansari MO, Uddin MK. Properties and application of MoS2 nanopowder: characterization, Congo red dye adsorption, and optimization. J Mater Res Technol J Mater Res Technol. 2021;13:1169–80. https://doi.org/10.1016/j.jmrt.2021.05.028.
6. Wang Y, Dai X, Zhan Y, Ding X, Wang M, Wang X. In situ growth of ZIF-8 nanoparticles on chitosan to form the hybrid nanocomposites for high-efficiency removal of Congo Red. Int J Biol Macromol. 2019;137:77–86. https://doi.org/10.1016/j.ijbiomac.2019.06.195.
7. Salah D, Hamd A, Soliman NK, Elzanaty AM, Alanazi AM, Shaban M, El-Sayed R, Ahmed SA. Polyaniline/glauconite nanocomposite adsorbent for congo red dye from textile wastewater. Separations. 2022;9(11):384. https://doi.org/10.3390/separations9110384.
8. Tibebe D, Negash A, Mulugeta M, Kassa Y, Moges Z, Yenealem D. Investigation of selected physico-chemical quality parameters in industrial wastewater by electrocoagulation process, Ethiopia. BMC Chem. 2022. https://doi.org/10.1186/s13065-022-00865-3.
9. Ruan W, Hu J, Qi J, Hou Y, Zhou C, Wei X. Removal of dyes from wastewater by nanomaterials: a review. Adv Mater Lett. 2019;10(1):9–20. https://doi.org/10.5185/amlett.2019.2148.
10. Madhav S, Ahamad A, Singh P, Mishra PK. A review of textile industry: Wet processing, environmental impacts, and effluent treatment methods. Environ Qual Manage. 2018;27(3):31–41. https://doi.org/10.1002/tqem.21538.
11. Achour Y, Bahsis L, Ablouh EH, Yazid H, Laamari MR, El Haddad M. Insight into adsorption mechanism of Congo red dye onto Bombax Buonopozense bark activated-carbon using Central composite design and DFT studies. Surfaces and interfaces. 2021;23: 100977.
12. Askari R, Mohammadi F, Moharrami A, Afshin S, Rashtbari Y, Vosoughi M, Dargahi A. Synthesis of activated carbon from cherry tree waste and its application in removing cationic red 14 dye from aqueous environments. Appl Water Sci. 2023. https://doi.org/10.1007/s13201-023-01899-1.
13. Harja M, Buema G, Bucur D. Recent advances in removal of Congo Red dye by adsorption using an industrial waste. Sci Rep. 2022. https://doi.org/10.1038/s41598-022-10093-3.
14. Han R, Ding D, Xu Y, Zou W, Wang Y, Li Y, Zou L. Use of rice husk for the adsorption of congo red from aqueous solution in column mode. Biores Technol. 2008;99(8):2938–46. https://doi.org/10.1016/J.BIORTECH.2007.06.027.
15. Chen H, Zhao J. Adsorption study for removal of Congo red anionic dye using organo-attapulgite. Adsorption. 2009;15(4):381–9. https://doi.org/10.1007/s10450-009-9155-z.
16. Rashtbari Y, Américo-Pinheiro JHP, Bahrami S, Fazlzadeh M, Arfaeinia H, Poureshgh Y. Efficiency of zeolite coated with zero-valent iron nanoparticles for removal of humic acid from aqueous solutions. Water Air Soil Pollution/Water Air Soil Pollut. 2020. https://doi.org/10.1007/s11270-020-04872-9.
17. Rummi DS. Textile Organic Dyes: Polluting effects and elimination methods from textile waste water. *Research India Publications*, *9*, 121–136. 2017.https://www.ripublication.com/ijcher17/ijcherv9n1_10.pdf
18. Alver E, Metin AL, Brouers F. Methylene blue adsorption on magnetic alginate/rice husk bio-composite. Int J Biol Macromol. 2020;154:104–13. https://doi.org/10.1016/j.ijbiomac.2020.02.330.

19. Malik A, Khan A, Anwar N, Naeem M. A comparative study of the adsorption of Congo red dye on rice husk, rice husk char and chemically modified rice husk char from aqueous media. Bull Chem Soc Ethiop. 2020;34(1):41–54.
20. Uddin MK. A review on the adsorption of heavy metals by clay minerals, with special focus on the past decade. Chem Eng J. 2017;308:438–62.
21. Awasthi A, Jadhao P, Kumari K. Clay nano-adsorbent: structures, applications and mechanism for water treatment. SN Appl Sci. 2019;1:1–21.
22. Mladenovic N, Makreski P, Tarbuk A, Grgic K, Boev B, Mirakovski D, Jordanov I. Improved dye removal ability of modified rice husk with effluent from alkaline scouring based on the circular economy concept. Processes. 2020;8(6):653.
23. Palapa NR, Normah N, Taher T, Mohadi R, Rachmat A, Lesbani A. Effectivity of indonesian rice husk as an adsorbent for removing congo red from aqueous solutions. Environ Nat Res J. 2021;19(4):225–65. https://doi.org/10.32526/ennrj/19/2020232.
24. Khana MI, Shanableha A, Elboughdirib N, Manzoord S, Mubeene S, Ur Rehmanf A. Application of NaOH modified rice husk as a potential sorbent for removal of Congo red from an aqueous solution. Desalin Water Treat. 2022;273:221–35.
25. Abou Alsoaud MM, Taher MA, Hamed AM, Elnouby MS, Omer AM. Reusable kaolin impregnated aminated chitosan composite beads for efficient removal of Congo red dye: Isotherms, kinetics and thermodynamics studies. Sci Rep. 2022;12(1):12972.
26. Adly ER, Shaban MS, El-Sherbeeny AM, Al Zoubi W, Abukhadra MR. Enhanced Congo red adsorption and photo-fenton oxidation over an iron-impeded geopolymer from ferruginous kaolinite: steric, energetic, oxidation, and synergetic studies. ACS Omega. 2022;7(35):31218–32.
27. Niu S, Xie X, Wang Z, Zheng L, Gao F, Miao Y. Enhanced removal performance for Congo red by coal-series kaolin with acid treatment. Environ Technol. 2021;42(10):1472–81.
28. Shaban M, Sayed MI, Shahien MG, Abukhadra MR, Ahmed ZM. Adsorption behavior of inorganic-and organic-modified kaolinite for Congo red dye from water, kinetic modeling, and equilibrium studies. J Sol-Gel Sci Technol. 2018;87:427–41.
29. Kausar A, Iqbal M, Javed A, Aftab K, Nazli ZIH, Bhatti HN, Nouren S. Dyes adsorption using clay and modified clay: a review. J Mol Liq. 2018;256:395–407. https://doi.org/10.1016/j.molliq.2018.02.034.
30. Ahmadfazeli A, Poureshgh Y, Rashtbari Y, Akbari H, Pourali P, Adibzadeh A. Removal of metronidazole antibiotic from aqueous solution by ammonia-modified activated carbon: adsorption isotherm and kinetic study. J Water Sanitation Hygiene Dev. 2021;11(6):1083–96. https://doi.org/10.2166/washdev.2021.117.
31. Stjepanović M, Velić N, Galić A, Kosović I, Jakovljević T, Habuda-Stanić M. From waste to biosorbent: removal of congo red from water by waste wood biomass. Water. 2021;13(3):279. https://doi.org/10.3390/w13030279.
32. Tuzen M, Sarı A, Saleh TA. Response surface optimization, kinetic and thermodynamic studies for effective removal of rhodamine B by magnetic AC/CeO2 nanocomposite. J Environ Manage. 2018;206:170–7.
33. Zhang Y, Zheng R, Zhao J, Ma F, Zhang Y, Meng Q. Characterization of H_3PO_4-treated rice husk adsorbent and adsorption of copper (II) from aqueous solution. BioMed Res Int. 2014. https://doi.org/10.1155/2014/496878.
34. Bamroongwongdee C, Suwannee S, Kongsomsaksiri M. Adsorption of Congo red from aqueous solution by surfactant-modified rice husk: Kinetic, isotherm and thermodynamic analysis. Songklanakarin J Sci Technol. 2019;41(5):1076–83. https://doi.org/10.1007/s10450-009-9155-z.
35. Aragaw TA, Angerasa FT. Synthesis and characterization of Ethiopian kaolin for the removal of basic yellow (BY 28) dye from aqueous solution as a potential adsorbent. Heliyon. 2020;6(9):e04975.
36. Chaari I, Fakhfakh E, Medhioub M, Jamoussi F. Comparative study on adsorption of cationic and anionic dyes by smectite rich natural clays. J Mol Struct. 2019;1179:672–7.
37. Aragaw TA, Alene AN. A comparative study of acidic, basic, and reactive dyes adsorption from aqueous solution onto kaolin adsorbent: effect of operating parameters, isotherms, kinetics, and thermodynamics. Emerg Contaminants. 2022;8:59–74. https://doi.org/10.1016/j.emcon.2022.01.002.
38. Tan TCN, Sen TK. Aqueous-phase methylene blue (MB) dye removal by mixture of eucalyptus bark (EB) biomass and kaolin clay (KC) adsorbents: kinetics, thermodynamics, and isotherm modeling. Sep Sci Technol. 2020;55(6):1036–50.
39. Jawad AH, Abdulhameed AS. Mesoporous Iraqi red kaolin clay as an efficient adsorbent for methylene blue dye: adsorption kinetic, isotherm and mechanism study. Surfaces and Interfaces. 2020;18: 100422.
40. Munagapati VS, Yarramuthi V, Kim Y, Lee KM, Kim DS. Removal of anionic dyes (reactive black 5 and Congo Red) from aqueous solutions using banana peel powder as an adsorbent. Ecotoxicol Environ Saf. 2018;148:601–7.
41. Abu TO, Adegoke HI, Odebunmi E, Shehzad M. Enhancing adsorption capacity of a kaolinite mineral through acid activation and manual blending with a 2:1 clay. https://journal.njtd.com.ng/index.php/njtd/article/view/2269. 2024.
42. Morimoto K, Tsuda K, Mizuno D. Literature review on the utilization of rice husks: focus on application of materials for digital fabrication. Materials. 2023;16(16):5597. https://doi.org/10.3390/ma16165597.
43. Hua Z, Pan Y, Hong Q. Adsorption of Congo red dye in water by orange peel biochar modified with CTAB. RSC Adv. 2023;13(18):12502–8. https://doi.org/10.1039/d3ra01444d.
44. Mohebali S, Bastani D, Shayesteh H. Equilibrium, kinetic and thermodynamic studies of a low-cost biosorbent for the removal of Congo red dye: acid and CTAB-acid modified celery (Apium graveolens). J Mol Struct. 2019;1176:181–93.
45. Ahmad R, Ansari K. Comparative study for adsorption of congo red and methylene blue dye on chitosan modified hybrid nanocomposite. Process Biochem. 2021;108:90–102.
46. Tofighy MA, Mohammadi T. Adsorption of divalent heavy metal ions from water using carbon nanotube sheets. J Hazard Mater. 2011;185(1):140–7. https://doi.org/10.1016/j.jhazmat.2010.09.008.
47. Safri A, Fletcher AJ, Safri R, Rasheed H. Integrated adsorption-photodegradation of organic pollutants by carbon Xerogel/Titania composites. Molecules/Mol Online/Mol Ann. 2022;27(23):8483. https://doi.org/10.3390/molecules27238483.
48. Klemes MJ, Skala LP, Ateia M, Trang B, Helbling DE, Dichtel WR. Polymerized molecular receptors as adsorbents to remove micropollutants from water. Acc Chem Res. 2020;53(10):2314–24. https://doi.org/10.1021/acs.accounts.0c00426.
49. Uddin MK, Rao RAK, Mouli KVC. The artificial neural network and Box-Behnken design for Cu2+ removal by the pottery sludge from water samples: Equilibrium, kinetic and thermodynamic studies. J Mol Liq. 2018;266:617–27.

50. Shaban M, Abukhadra MR, Hamd A, Amin RR, Khalek AA. Photocatalytic removal of Congo red dye using MCM-48/Ni2O3 composite synthesized based on silica gel extracted from rice husk ash; fabrication and application. J Environ Manage. 2017;204:189–99.
51. Rose PK, Poonia V, Kumar R, Kataria N, Sharma P, Lamba J, Bhattacharya P. Congo red dye removal using modified banana leaves: adsorption equilibrium, kinetics, and reusability analysis. Groundw Sustain Dev. 2023;23: 101005.
52. Al-Salihi S, Jasim AM, Fidalgo MM, Xing Y. Removal of Congo red dyes from aqueous solutions by porous γ-alumina nanoshells. Chemosphere. 2022;286: 131769.
53. Ayawei N, Ebelegi AN, Wankasi D. Modelling and interpretation of adsorption isotherms. J Chem. 2017. https://doi.org/10.1155/2017/3039817.
54. Foo K, Hameed B. Insights into the modeling of adsorption isotherm systems. Chem Eng J. 2010;156(1):2–10. https://doi.org/10.1016/j.cej.2009.09.013.
55. Altalhi TA, Ibrahim MM, Mersal GA, Mahmoud M, Kumeria T, El-Desouky MG, El-Bindary AA, El-Bindary MA. Adsorption of doxorubicin hydrochloride onto thermally treated green adsorbent: equilibrium, kinetic and thermodynamic studies. J Mol Struct. 2022;1263: 133160. https://doi.org/10.1016/j.molstruc.2022.133160.
56. Meléndez-Ortiz HI, Puente-Urbina B, Mercado-Silva JA, García-Uriostegui L. Adsorption performance of mesoporous silicas towards a cationic dye. Influence of mesostructure on adsorption capacity. Int J Appl Ceramic Technol. 2019;16(4):1533–43.
57. Zhou Y, Ge L, Fan N, Xia M. Adsorption of Congo red from aqueous solution onto shrimp shell powder. Adsorpt Sci Technol. 2018;36(5–6):1310–30.
58. Ho YS. Review of second-order models for adsorption systems. J Hazard Mater. 2006;136(3):681–9.
59. Cheng Z, Zhang L, Guo X, Jiang X, Li T. Adsorption behavior of direct red 80 and congo red onto activated carbon/surfactant: process optimization, kinetics and equilibrium. Spectrochim Acta Part A Mol Biomol Spectrosc. 2015;137:1126–43.
60. Lafi R, Montasser I, Hafiane A. Adsorption of congo red dye from aqueous solutions by prepared activated carbon with oxygen-containing functional groups and its regeneration. Adsorpt Sci Technol. 2019;37(1–2):160–81.
61. Parvin S, Biswas BK, Rahman MA, Rahman MH, Anik MS, Uddin MR. Study on adsorption of Congo red onto chemically modified egg shell membrane. Chemosphere. 2019;236: 124326.
62. Kwikima MM, Chebude Y, Meshesha BT. Kinetics, adsorption isotherms, thermodynamics, and desorption studies of cadmium removal from aqueous solutions using bamboo sawdust/rice husk biochar. Biomass Conv Biorefin. 2022;13(11):9367–79. https://doi.org/10.1007/s13399-022-03472-3.
63. Askari R, Afshin S, Rashtbari Y, Moharrami A, Mohammadi F, Vosuoghi M, Dargahi A. Synthesis of activated carbon from walnut wood and magnetized with cobalt ferrite ($CoFe^2O_4$) and its application in removal of cephalexin from aqueous solutions. J Dispersion Sci Technol. 2021;44(7):1183–94. https://doi.org/10.1080/01932691.2021.2008421.
64. Rashtbari Y, Afshin S, Hamzezadeh A, Gholizadeh A, Ansari FJ, Poureshgh Y, Fazlzadeh M. Green synthesis of zinc oxide nanoparticles loaded on activated carbon prepared from walnut peel extract for the removal of Eosin Y and Erythrosine B dyes from aqueous solution: experimental approaches, kinetics models, and thermodynamic studies. Environ Sci Pollut Res Int. 2021;29(4):5194–206. https://doi.org/10.1007/s11356-021-16006-7.